Mick, E., Stix, J. and Avard, G. (2026) "The Origin of Fresh Glass in Phreatic Eruptions at Rincón de la Vieja and Turrialba Volcanoes, Costa Rica: Secondary Hydration within Hydrothermal Systems", Volcanica, 9(1). doi: 10.30909/vol/jysr2288.

The Origin of Fresh Glass in Phreatic Eruptions at Rincón de la Vieja and Turrialba Volcanoes, Costa Rica: Secondary Hydration within Hydrothermal Systems

Emily Mick - Department of Earth and Planetary Sciences, McGill University, 3450 University Street, Montreal, QC H3A 0E8, Canada; Strasbourg Institute of Earth & Environment (ITES), 5 rue René Descartes, Strasbourg 67084, France

Geoffroy Avard - Observatorio Volcanológico y Sismológico de Costa Rica (OVSICORI), Universidad Nacional, Campus Omar Dengo, Apartado Postal 2386-3000 Heredia, Costa Rica

John Stix - Department of Earth and Planetary Sciences, McGill University, 3450 University Street, Montreal, QC H3A 0E8, Canada

Corresponding author: Emily Mick – emily.mick@mail.mcgill.ca

Keywords: Turrialba volcano, Rincón de la Vieja volcano, secondary hydration, phreatic eruptions, volcanic glass, hydrogen isotope ratios (δD)

Abstract

Despite involving no fresh magma, phreatic eruptions are increasingly found to contain juvenile material. This study examines ash from phreatic eruptions at Turrialba and Rincón de la Vieja volcanoes (Costa Rica) to determine whether volcanic glass originates from new magma input or shallow stalled magma passively entrained. Hydrogen isotope ratios (δD) and water speciation (OH/H_2O_{mol}) are used to distinguish fresh magmatic from rehydrated glasses. At Rincón de la Vieja, glasses contain up to 0.71 wt.% H_2O_{total} with δD values between –27‰ and –3‰, well above the magmatic degassing trend consistent with secondary hydration by a hydrothermal source. Turrialba samples show a mixed signal; six samples fall within magmatic δD and water values, while three exhibit δD values from –99‰ to –104‰ and elevated H_2O contents up to 2.29 wt.%, consistent with secondary hydration by a hydrothermal source. These results suggest the shallow storage of magma entrained during purely phreatic eruptions.

1 Introduction

Phreatic eruptions result from the explosive expansion of groundwater following input of magmatic heat and/or fluids but are not driven by the fragmentation of fresh magma (Barberi et al., 1992). In contrast, phreatomagmatic eruptions involve both the explosive expansion of groundwater and fresh magma (i.e., juvenile material) (Barberi et al., 1992). Despite this, juvenile material has increasingly been identified in phreatic eruptions, calling into question their classification. A re-examination of ash produced during the precursory 1980 eruptions of Mount St. Helens, USA, was the first instance of juvenile glass identified in phreatic ash (Cashman and Hoblitt, 2004). Examination of ash erupted up to two months before the catastrophic eruption on May 18, 1980, revealed small amounts of juvenile material from a cryptodome, up to 4%, produced by eruptions previously identified as phreatic (Cashman and Hoblitt, 2004). Two more recent, notable examples are the 2012 eruption of Tongariro volcano and the 2014 eruption of Ontake volcano. The 2012 eruption of Tongariro, New Zealand, was caused by the sudden decompression of a sealed hydrothermal system following a landslide (Pardo et al., 2014). This produced a 7-kilometer plume with significant juvenile material, ascribed to recycling of older glassy material or the excavation of a recently intruded dike (Lube et al., 2014; Pardo et al., 2014). Similarly, the 2014 eruption of Ontake, Japan, resulted from the rupture of a hydrothermal seal, leading to a 7-kilometer plume and pyroclastic density currents (Kaneko et al., 2016). Shallow magma (>3 km deep) provided heat and juvenile material for the eruption (Miyagi et al., 2020). Both these eruptions are classified as phreatic despite containing up to 15% juvenile material (Miyagi et al., 2020; Pardo et al., 2014).

Despite increasing recognition of juvenile material in phreatic eruptions, volcanologists remain cautious about reclassifying these events as phreatomagmatic due to uncertainty regarding the origin of the juvenile material (e.g., Pardo et al., 2014). This study seeks to understand the role of fresh glass in eruptions classified as phreatic. To do so, we examine ash samples from phreatic eruptions at Turrialba and Rincón de la Vieja volcanoes in Costa Rica (Figure 1), where frequent eruptive activity has occurred over the period of study (Turrialba: 2014-2022; Rincón de la Vieja: 2017-2021). While phreatic eruptions, by definition, do not contain juvenile material, both Turrialba and Rincón de la Vieja have produced

seemingly juvenile material, raising key scientific questions which we address in this paper (Battaglia et al., 2019; de Moor et al., 2016).It is crucial to determine whether juvenile material results from new, active magma or from entrained, stalled magma. This distinction is key to forecasting future eruptions; the presence of juvenile material in eruptions may indicate the movement of fresh magma within a volcanic system, potentially signaling increasing activity and greater eruption hazard (Barberi et al., 1992; Stix and de Moor, 2018; Germanovich and Lowell, 1995). Magma, whether solidified or otherwise, that is passively entrained during a phreatic eruption likely resides within the shallow subsurface before eruption (Stix and de Moor, 2018). If the volcanic edifice also contains a hydrothermal system, as is the case for the two volcanoes in this study, the magma body is likely to interact with it. To differentiate passive magma from active magma, we use secondary hydration as a tool to distinguish fresh glass from magmatic material stalled within the hydrothermal system. Here, secondary hydration refers specifically to pre-eruptive hydration of glass through interaction with the elevated temperatures of the hydrothermal system, rather than post-eruptive hydration at ambient conditions.

1.1 Secondary Hydration

Water plays an important role in volcanic environments and is broadly considered the most important volatile in volcanic eruptions (e.g., Silver and Stopler, 1989; Inhinger et al., 1999; Newman and Lowenstern, 2002; Newman et al., 1988; Giachetti et al., 2015; Hudak and Bindeman, 2020). Water occurs as two species, hydroxyl (OH) and molecular water (H_2O_{mol}) which together comprise the total water content of a magma (H_2O_{total}). Previous studies have carefully documented the behaviour of water during degassing, finding that molecular water is the primary diffusive species due to weaker hydrogen bonds as opposed to the stronger Si-OH bonds of hydroxyl (Seligman et al., 2016 and references therein). Furthermore, at high temperatures, molecular water can repartition to hydroxyl leading to further dehydration (Hudak et al., 2022). In addition to a loss of H_2O_{mol}, deuterium becomes depleted during degassing as diffusive molecular water favours the heavier isotope (^2H) while hydroxyl favours the lighter isotope (^1H) of hydrogen (Newman et al., 1988; Zhang et al., 1991; Dobson et al., 1989; Giachetti et al., 2020; Seligman et al., 2016). If unaltered, the water content, speciation,

and isotopic composition of juvenile eruptive products reflect their magmatic origin, following a defined magmatic degassing trend (Taylor et al.,1983; Newman et al., 1988).

Secondary hydration or rehydration of magmatic glass occurs due to water uptake by pre-, syn-, or post-eruptive glass be it meteoric water or other (e.g., hydrothermal fluids). Following degassing magmatic water occurs primarily in the form of OH while meteoric water is predominantly H_2O_{mol}, allowing for the discrimination between primary and secondary water. While magmatic degassing produces a single well-defined trend in terms of δD, rehydration is controlled by the isotopic signature of the rehydrating water, usually the local meteoric water (Newman et al., 1988; Dobson et al., 1989; Giachetti et al., 2020; Seligman et al., 2016). Post-eruptive rehydration at atmospheric conditions typically produces an offset of -29 to -31‰, with the glass being isotopically lighter than the rehydrating water (Seligman et al., 2016 and references therein). However, this fractionation is primarily controlled by temperature, with hydration occurring faster at higher temperatures (Hudak et al., 2022 and references therein). At elevated temperatures and pressures, such as those found within a hydrothermal system, rehydration occurs first through ion exchange of OH with soluble ions (e.g., Na^+), followed by absorption of molecular water (Seligman et al., 2016). Hydrothermal fluids are composed primarily of meteoric water with a lesser component of upwelling magmatic water and as a result have an intermediate isotopic composition.

A key consideration is whether any post-eruptive rehydration may have occurred, thereby compromising the pre-eruptive isotopic signature. Studies show that ambient-temperature rehydration takes thousands of years. At Mount St. Helens, a comparison of samples collected immediately after the 1980 eruption with those sampled 35 years later revealed no significant rehydration, except in cases of fumarolic exposure where elevated temperatures accelerated rehydration (Seligman et al., 2018). Hence, we are confident our samples collected in the days, weeks or months following eruption retain their pre-emplacement chemistry.

1.2 Geologic Setting

Turrialba is a basaltic to andesitic stratovolcano dating to the Holocene, with a minimum age of 9300 years B.P. (Figure 1b; Martini et al., 2010; Reagan et al., 2006). It is part of the Central

American Volcanic Arc (CAVA), formed by the subduction of the Cocos Plate beneath the Caribbean Plate at a low angle and high temperature (de Moor et al., 2016). Turrialba also hosts a complex magmatic-hydrothermal system (de Moor et al., 2016). The last magmatic eruption at Turrialba occurred between 1864-1866; following a period of quiescence the volcano re-activated in 1996 and has been restless ever since (de Moor et al., 2016; Martini et al., 2010). In 2014 Turrialba entered a new phase of heightened activity marked by nearly continuous degassing and frequent ash emissions. Current activity at Turrialba is characterized as phreatic (Alvarado et al., 2016).

Rincón de la Vieja is an active andesitic volcanic complex in the Guanacaste volcanic range, also part of the Central American Volcanic Arc (Figure 1c; Carr, 1984). The most recent magmatic eruption occurred in 1967, since which time activity has been primarily phreatic to phreatomagmatic (Alvarado et al., 1992, Boudon et al., 1996). The volcano entered a quiescent period in 1998, which lasted until 2011 (Global Volcanism Program, 2016). Activity surged again in 2014, peaking in March 2016 with 220 eruptions recorded in a single month (Battaglia et al., 2019). Rincón de la Vieja hosts a complex magmatic-hydrothermal system, of which a hyper-acidic crater lake is the most visible expression (Battaglia et al., 2019; Global Volcanism Program, 2016). Rincón de la Vieja remains active at the time of writing in March 2026, producing phreatic and phreatomagmatic eruptions in addition to near-constant degassing (Global Volcanism Program, 2022; Global Volcanism Program, 2023a; Global Volcanism Program, 2023b; Global Volcanism Program, 2024).

1.3 Comparing Two Volcanic Systems

This study compares two distinct volcanic systems: Rincón de la Vieja and Turrialba, with a focus on glassy erupted material and secondary hydration. These systems share several key similarities, such as their inclusion in the Central American Volcanic Arc and their proximity, only 200 km apart, with both experiencing tropical climates (Figure 1; Battaglia et al., 2019; de Moor et al., 2016). Despite this, their meteoric water isotopic signatures differ (Rincón de la Vieja +26‰ δD; Turrialba -115.9‰ to +13.7‰ δD; IAEA/WMO, 2015; Sanchez-Murillo et al., 2016), which is crucial for differentiating secondary hydration (Seligman et al., 2016).

While both systems host active magmatic-hydrothermal systems, only Rincón de la Vieja hosts a crater lake (Figure 1c; Global Volcanism Program, 2016). Another important distinction between the systems is the visual observation of fresh magma in the vent at Turrialba during the period of study but not at Rincón de la Vieja (Global Volcanism Program, 2018). Despite this, fresh glass has been identified in both systems (Battaglia et al., 2019; de Moor et al., 2016). In addition, the sample suites from each system were collected during periods of high activity, 2014-2016 for Turrialba and 2020-2021 for Rincón de la Vieja, allowing for the comparison between the systems during similar phases of activity (Global Volcanism Program, 2015, 2017a, 2020, 2021). Importantly, phreatic activity at both Turrialba and Rincón de la Vieja is attributed to repeated instances of hydrothermal sealing (Battaglia et al., 2019; Mick et al., 2021). Sealing occurs when hydrothermal minerals precipitate from fluids, blocking permeable pathways and reducing permeability (Heap et al., 2017; Stix and de Moor, 2018). As gas accumulates below the seal, pressure builds until it ruptures, triggering a phreatic eruption (Christenson et al., 2010).

2 Methods and Materials

This study utilizes ash samples from Turrialba erupted between 2014 and 2022 and from Rincón de la Vieja erupted between 2017 and 2021. Turrialba samples are from eruptions on October 31, 2014, May 6, 2015, October 26, 2015, May 25, 2016, October 3, 2016, March 9, 2017, and January 18, 2022. With the exception of the sample collected January 18, 2022, all samples from Turrialba were collected on the day of eruption or in the few days following eruptions by GA or local community members. The sample erupted January 18, 2022, was collected May 18, 2022, but we are confident of the date of eruption. The suite of samples from Rincón de la Vieja was collected from eruptions on May 23, 2017, January 20, 2019, January 28, 2020, January 30, 2020, April 19, 2020, and June 28, 2021. All samples from Rincón de la Vieja were collected on the day of eruption for GA by local community members.

2.1 Sample Preparation

Samples were washed to remove adhering particles from grain surfaces and dried overnight at 40°C. Samples were then sieved into four size fractions: <63 µm, 63 µm-125 µm, 250 µm-

500 µm, and >500 µm. Grain counting was completed for the 250 µm-500 µm and >500 µm size fractions. Grains were classified as free crystals, lithic fragments, accretionary pellets, hydrothermal grains or glassy fragments following the scheme set out by Romero et al. (2020). Glassy grains and free crystals were mounted in epoxy and polished for further analysis. Only fresh-looking glass was used in subsequent analysis.

2.2 Scanning Electron Microscope (SEM)

Epoxy grain mounts were carbon-coated before SEM analysis, which was performed using a Hitachi SU5000 equipped with an energy dispersive X-ray spectrometer (EDS) at McGill University. Operating conditions included 15 kV beam energy, 20 nA beam current, spot intensity of 50, and a working distance (Z) of 10 mm. EDS analysis and data processing were conducted using Oxford Instruments' Aztec software. The SEM was used for phase discrimination of fresh-looking glass and free crystals. Electron back scatter diffraction (EBSD) images were acquired for all grains.

2.3 Electron Probe Microanalysis (EPMA)

Glasses identified using SEM were further analyzed using electron probe microanalysis. Previously prepared carbon coated mounts were analyzed using a Cameca SX100 electron microprobe equipped with five wavelength dispersive spectrometers at McGill University. Major elements were analyzed with a beam diameter of 10 µm, a voltage of 20 kV and a current of 5 nA. Standards were pantellerite obsidian (Na, Si, Al, K), basaltic glass (Mg, Ca, Ti, Fe), and spessartine (Mn).

2.4 Fourier-Transform Infrared Spectroscopy (FTIR-ATR)

Fourier-transform infrared spectroscopy with attenuated total reflectance (FTIR-ATR) was performed at the US Geological Survey Cascades Volcano Observatory using a Nicolet iN10 microscope and OMNIC software. Prior to analysis, carbon coating was removed by polishing. The microscope was equipped with a Ge crystal and cooled with liquid nitrogen. Measurements were taken at a pressure setting of 15 over a wavenumber range of 675–4000 cm^{-1}. Standards were analyzed using a 100 µm×100 µm aperture, while glasses were analyzed

using a 50 µm×50 µm aperture. Each spectrum consisted of 64 scans at normal resolution with a scan time of 12 seconds. Standard data and calibration curves are available in supplementary materials Figures 1-3 and Table 3. Data processing was conducted using the procedure set out by Lowenstern and Pitcher (2013). Total water and molecular water were calculated using the following formula:

$$wt.\%\ H_2O = \left(\omega \times \frac{A}{\rho}\right) + b$$

where *A* is the peak height in absorbance units at 3450 cm^{-1} for H_2O_{total} and 1630 cm^{-1} for H_2O_{mol}. The density normalized correction factor is represented by ω, ρ is density and *b* is the x-intercept as set out in Lowenstern and Pitcher (2013). For H_2O_{total} at 3450 cm^{-1} ω is 550. For H_2O_{mol} at 1630 cm^{-1} ω is 525. The hydroxyl content (OH) was calculated by the difference between total water and molecular water.

2.5 Secondary Ion Mass Spectrometry (SIMS)

Glasses were analyzed for hydrogen isotopes at Woods Hole Oceanographic Institution using a Cameca IMS 1280 ion microprobe. Prior to analysis, grains were removed from epoxy and mounted in indium due to the risk of epoxy outgassing creating a high water background. Mounts were then gold-coated and placed under vacuum overnight. SIMS analysis was done on glasses >500 µm at their largest dimension, although much smaller areas were exposed after mounting. Points were chosen as far as possible from bubble/vesicle walls. Ionisation was achieved using a primary beam of Cs^+ ions, accelerated at 10 kV, with a diameter of 20 µm and a current of 0.59-0.84 nA. The field aperture was set to 2000 µm to maximize counts on the electron multiplier detector. Each analysis consisted of 30 cycles of peak counting with count times of 3 seconds for $^{16}O^1H$ and 15 seconds for $^{16}O^2H$. Suprasil glass with 0 wt.% water was used to verify negligible background levels. Standard data is available in supplementary materials Table 5.

3 Results

3.1 Ash Componentry

Ash was characterized in terms of its components using categories set out by Romero et al. (2020). Two fractions of each sample, 250 µm-500 µm and >500 µm, were characterized in terms of componentry, and these results are presented in Table 1 and Figure 2. Grains were classified as 1) fresh glass, 2) hydrothermal grains, 3) accretionary pellets, 4) lithics, or 5) free crystals. Descriptions of each category follow:

1. **Fresh glass** appeared dark brown to black, with vitreous surfaces and no visible alteration. Grains were typically angular, and some contained visible microlites. Microlites identified by SEM included plagioclase, olivine, clinopyroxene, and orthopyroxene, with minor amounts of ilmenite, magnetite, and apatite. Textures ranged from blocky to highly vesicular (Figure 3). Blocky grains generally contained more microlites.

2. **Hydrothermal grains** exhibited a wide variety of colors, including white, yellow, orange, pink, and red. Alteration ranged from partial to complete. Grains were blocky and vesicular and ranged from angular to rounded. Vesicular grains occasionally showed filling of vesicles in addition to alteration.

3. **Accretionary pellets** were spherical aggregates composed of very fine ash particles, loosely bound. Some pellets had a larger ash grain as a nucleus. These are typical of wet eruptions and occurred predominantly during the wet season (Gilbert and Lane, 1994).

4. **Lithic fragments** were grey to black angular fragments of previously erupted material. Lithics were non-vesicular. Some grains had minor surface alteration, but lithics were largely unaltered.

5. **Free crystals** included individual crystals or fragments, occasionally with small amounts of adhered glass. Crystals were generally angular, with few euhedral examples, and included plagioclase, olivine, clinopyroxene, and orthopyroxene.

With the exception of sample TA-6 which contained no glass and sample TA-4 which contained glass only in the 250 µm - 500 µm fraction, all samples contain some proportion of glass regardless of grain size. In addition, glass is consistently more abundant in the smaller size fraction, potentially due to breakage of fragile vesicular material (Figure 3). All samples containing glass had variable proportions of both blocky and vesicular grains regardless of source volcano. Microlites were predominantly acicular plagioclase crystals.

Microlite content and composition did not vary significantly between volcanoes. Textures varied from blocky to highly vesicular and were independent of composition. Importantly, glass was vitreous with no visible alteration, i.e., milky surfaces (Figure 3). Of note is the variation of glass within samples. Samples from individual eruptions could contain both highly vesicular and blocky grains in addition to highly variable microlite contents across single samples. When considering Turrialba and Rincón de la Vieja separately, visual analysis of the glass shows no significant differences between the two systems.

3.2 Major Element Oxides

To determine if glass grains are in fact fresh, we first considered whether they represent magmatic major oxide compositions or if they have undergone some degree of alteration. We analyzed only glassy grains. Samples for Rincón de la Vieja contained 56.70 to 72.24 wt.% SiO_2 (Table 2; Figure 4), corresponding with broadly andesitic to rhyolitic compositions. In contrast, samples from Turrialba contained 52.64 to 64.05 wt.% SiO_2 corresponding to a less evolved, basaltic andesite to andesitic composition (Le Bas et al., 1986)

To assess whether these compositions follow expected magmatic differentiation trends, we compare our data to typical geochemical systematics of arc magmas (Pearce and Peate, 1995). In such systems, fractional crystallization generally produces increasing SiO_2 in the magma accompanied by decreasing MgO and CaO with more variable behaviour in Fe_2O_3 and alkalis depending on crystallizing phases. Most samples follow broadly coherent trends consistent with magmatic differentiation (Figure 4). For both Rincón de la Vieja and Turrialba, the most significant deviation from magmatic trends occurs for Al_2O_3 where values are up to several weight percent above expected magmatic values. Elevated aluminum values may be due to

fine plagioclase microlites within the glass; this is supported by elevated values of Na_2O in these samples (Table 2). Minor deviations of ± 2 wt.% from magmatic trends are also seen for Fe_2O_3 at both Turrialba and Rincón de la Vieja in addition to K_2O at Turrialba.

3.3 Deuterium Isotopic Measurements

The behaviour of hydrogen isotopes is well documented during magmatic degassing and has been previously applied to identify fresh magmatic material (e.g., Giachetti et al., 2020; Dobson et al., 1989; Newman et al., 1988). It is possible to use hydrogen isotopic contents in conjunction with water contents as a discriminatory tool due to the speciation of water and isotopic fractionation during degassing. As discussed above, H_2O_{mol} is the primary diffusive species during magmatic degassing and favours heavier isotopes leading to a depletion in deuterium during degassing (Giachetti et al., 2020; Seligman et al., 2016). A reference magmatic degassing trend was constructed using relationships between δD and H_2O_{total} derived from Giachetti et al. (2020), Taylor et al. (1983) and Newman et al. (1988) and is shown in Figure 5.

Looking first at Turrialba we see a significant spread in values. Deuterium isotopic values vary from -102‰ to -61‰ while total water content varies from 0.19 to 2.91 wt.% (Table 3). Six samples fall within the magmatic degassing trend while three samples fall below the magmatic degassing trend (Figure 5). We propose that these three samples represent a secondary hydration trend, which will be discussed in section 4.2. Samples from Rincón de la Vieja plot in a tightly packed cluster above all Turrialba values and the magmatic degassing trend. Deuterium isotopic values vary from -27‰ to -3‰ while total water content varies from 0.18 to 0.71 wt.% (Table 3). None of the samples from Rincón de la Vieja fall within the magmatic degassing trend, and we propose that all represent secondary hydration by a single source distinct from the Turrialba source (Figure 5).

3.4 Water Speciation

In magma, water is present as OH and H_2O_{mol} which together comprise the total water content (H_2O_{total}). The behaviour of the two species in magmatic degassing is well documented, where

H_2O_{mol} acts as the diffusive species, and the relative proportion of water species in a sample can be used to evaluate the magmatic origin of a sample. A reference magmatic degassing trend was constructed using relationships between OH/H_2O_{mol} and H_2O_{total} derived from Giachetti et al. (2020) and Newman et al. (1988) with data recalculated to a consistent basis for comparison (Figure 6). The magmatic trend shows that loss of water through degassing causes a gradual increase in the OH/H_2O_{mol} ratio down to 1 wt.% water, at which point the ratio increases quickly as OH begins to diffuse.

Most samples from Turrialba fall within the defined magmatic trend while five fall above it (Figure 6). Of the five samples falling off the magmatic degassing trend, one sample corresponds to the hydrated samples shown in Figure 5, and 2 samples correspond to the magmatic degassing trend in Figure 5. We were unable to obtain isotopic measurements for the final two samples. There is thus poor agreement between Figures 5 and 6 in terms of which samples exhibit magmatic degassing and which show rehydration. Total water content varies from 0.19 to 2.91 wt.%, molecular water varies from 0.03 to 1.38 wt.%, and hydroxyl from 0.16 to 1.78 wt.% (Table 3). Samples from Rincón de la Vieja fall largely within the magmatic degassing trend, in contrast to our isotopic results (Figures 5, 6). Total water content varies from 0.18 to 0.71 wt.%, molecular water varies from 0.02 to 0.41 wt.%, and hydroxyl from 0.05 to 0.58 wt.% (Table 3). Of the samples analyzed for water speciation, only two samples fall above the defined magmatic degassing trend, indicating that most Rincón de la Vieja samples appear to represent fresh magmatic material, again reflecting poor agreement between isotope and speciation methods.

4 Discussion

4.1 Textural and Compositional Interpretations

Based on compositional and textural analyses, the volcanic glass samples from both Turrialba and Rincón de la Vieja appear fresh. No visible signs of alteration are present, and this observation is supported by electron microprobe (EPMA) data. If the glass were recycled material, one would expect to see evidence of alteration in the glass matrix or associated phenocrysts which is absent in all cases. Alteration might include secondary mineral

precipitates on glass surfaces, the formation of an altered shell layer, and the replacement of primary minerals by hydrothermal phases (Cassel and Breecker, 2017). The presence of well-formed phenocrysts and microlites indicates relatively slow cooling, a texture not typically produced by the rapid quenching associated with explosive fragmentation of active magma (Hammer et al., 1999).

Of note is an apparent evolution in magmatic composition at Rincón de la Vieja between January 2019 and June 2021. Samples erupted January 20, 2019, represent the least evolved endmember with values of SiO_2 between 56 and 61 wt.% (Table 2). Samples erupted January 28, 2020, and January 30, 2020, show significantly greater spread and represent intermediate values (59 to 69 wt.% SiO_2). Samples erupted April 19, 2020, are more evolved with SiO_2 values of 62 to 66 wt.%. Finally, ash erupted June 28, 2021, appears most evolved with 64 to 72 wt.% SiO_2 (Figure 4). This trend may reflect the evolution of a single magma body sourced by each of these eruptions, or several magma bodies at different stages of differentiation although we believe this to be less likely because of the systematic compositional changes with time. Conversely, no temporal trend is seen at Turrialba.

4.2 Isotopic Indicators of Secondary Hydration

Secondary hydration occurs when glass is re-hydrated by local waters after magmatic degassing (Giachetti et al., 2020; Seligman et al., 2016). Over the course of hundreds to thousands of years, glass may rehydrate to an equilibrium value of approximately 4wt.% H_2O_{total} (Nolan and Bindeman, 2013). The hydrogen isotopic distinction between magmatic and meteoric waters allows differentiation between primary magmatic water and secondary hydration. Using data from Giachetti et al. (2020), Newman et al. (1988) and Taylor et al. (1983), we show the known magmatic degassing trend in Figure 5. This trend, initially presented by Taylor et al. (1983), characterizes magmatic degassing during open system conditions. In contrast, closed-system degassing, where magma remains in contact with the exsolved vapor phase, does not lead to the same degree of progressive deuterium depletion (De Hoog et al., 2009). Both Turrialba and Rincón de la Vieja are open systems throughout the period of study as indicated by their near constant degassing and the presence of a near-continuous plume over their main vents. During rehydration, it has been shown that hydrogen

isotopic values of glass will proceed towards the hydrating water isotopic values (e.g., Seligman et al., 2016; Friedman et al., 1993a; Friedman et al., 1993b; Anovitz et al., 2009; Nolan and Bindeman, 2013). Due to isotopic fractionation, glass will remain depleted compared to rehydrating water; at atmospheric conditions felsic glasses show a relative depletion of -33‰ while mafic glasses show a relative depletion of -23‰ in experimental conditions. More generally, values of -30 to -35‰ δD are accepted for post-eruptive rehydration of volcanic glasses (Martin et al., 2017). With increasing temperature, the degree of fractionation between the glass and rehydration water has been shown to decrease (Hudak et al., 2022).

Initial magmatic water compositions shown in Figure 5 are derived from melt inclusions in olivine and pyroxene. Although no direct studies are available for Turrialba and Rincón de la Vieja, data from the Mariana Arc provide a useful analogue, as this setting is governed by the same process of slab dehydration (Shaw et al., 2008). Shaw et al. (2008) report values of -12 to -55‰ δD, which are taken here as representative of slab derived magmatic fluids. Turrialba exhibits a strong mantle signature and therefore a relatively weak contribution from slab-derived fluids, suggesting that the more depleted end of the range is more appropriate for Turrialba, whereas Rincón de la Vieja is likely characterized by less depleted values (de Moor et al., 2016). Using these constraints as initial compositions, proposed rehydration trends were inferred.

Applying these criteria, some Turrialba glass samples reflect fresh magmatic degassing, while others exhibit evidence of secondary hydration (Figure 5). Specifically, samples TA-1-6 and TA-1-7 (October 31, 2014), as well as TA-7-5 (October 3, 2016) lie outside the magmatic degassing trend defined by δD and total water content. Instead, they follow a trend consistent with the isotopic signature of hydrothermal fluids. Vaselli et al., (2010) measured fumarole gases and found δD values of -94.3 to -55.1‰. As fumaroles are surface expressions of a hydrothermal system that is impossible to sample at depth, we assume that fumarolic values are representative of the sub-surface hydrothermal system. Based on these findings, we propose a rehydration trend for Turrialba glass, illustrated in Figure 5. As we have determined that post-eruptive rehydration was not possible given that sampling occurred immediately

following eruptions, we conclude that the rehydration was pre-eruptive. Samples having undergone pre-eruption secondary hydration are indicative of solidified or semi-solidified magma stored within and interacting with the shallow hydrothermal system and hence, likely passively entrained during phreatic events. In contrast, samples within the magmatic degassing trend indicate active, fresh magma likely associated with phreatomagmatic eruptions. While these samples fall along the magmatic degassing trend, we acknowledge that rehydration by relatively high-δD fluids could potentially produce a similar isotopic signature. However, the coherence of the trend with established degassing trajectories, together with the lack of independent evidence for late-stage hydration, supports a primary magmatic origin of these samples.

In contrast, none of the seemingly fresh Rincón de la Vieja glass samples retain isotopic signatures of magmatic degassing (Figure 5). Instead, all samples fall above the magmatic trend in a tight cluster at comparatively low water contents. Although direct sampling of the hydrothermal fluids interacting with stored magma is not possible, we propose that the crater lake filling the main vent of the volcano is broadly representative of the hydrothermal system below in terms of hydrogen isotopes. The crater lake has δD values of -6.4 to +8.3‰ while the glass samples have an average value of -11‰ (Tassi et al., 2009). At Rincón de la Vieja local meteoric water has been measured at +26‰ (IAEA/WMO, 2015). Secondary hydration by crater lake water accounts for the isotopic composition found in the glasses, yielding a maximum fractionation of -19‰ between the glass and water. Based on these results, we propose the secondary hydration trend for Rincón de la Vieja presented in Figure 5.

Building on this interpretation, we propose the following sequence applicable to both volcanoes: (1) magma ascends and undergoes degassing and partial cooling at shallow depth, forming a solid or semi-solid glassy material; (2) this stalled magma resides within the hydrothermal system, where it interacts with hydrothermal fluids and undergoes secondary hydration prior to eruption; (3) during a phreatic eruption, this pre-existing, rehydrated glass is fragmented and passively entrained in the eruptive products.

Temperature exerts a primary control on volcanic glass rehydration by influencing water diffusion rates, solubility and isotopic fractionation. Diffusion is especially temperature-

sensitive, increasing exponentially at higher temperatures (Hudak and Bindeman, 2020; Hudak et al., 2021). This makes high temperature pre-eruptive interactions between water and glass more significant in terms of hydration than post-depositional interactions. At hydrothermal temperatures (175 °C to 375 °C), diffusivity will be orders of magnitude higher than at surface conditions (Martin et al., 2017). For example, the hydration front was found to move 1 μm every 100 years at 20°C while at 75°C it moved the same distance in only 2 years (Martin et al., 2017). Temperature also affects how much water can be incorporated by a glass. Hydrothermal experiments have linked increasing temperature to increasing solubility, 2.75 wt.% at 175 °C compared to 4.1 wt.% at 375 °C (Hudak and Bindeman, 2020). In addition, isotopic fractionation is reduced at elevated temperatures (Seligman et al., 2018).

4.3 Speciation Indicators of Secondary Hydration

To this point, we have applied hydrogen isotopes in identifying magmatic degassing and secondary hydration. Water speciation has also been characterized during magmatic degassing. Using data from Giachetti et al. (2020) and Newman et al. (1988), we define a magmatic degassing trend shown in Figure 6. Based on findings from Martin et al. (2017), we expect to see increased total water and OH/H_2O_{mol} during rehydration. Although our data largely fall within the magmatic trend, speciation results do not align with hydrogen isotope interpretations (Figure 5).

Considering first Rincón de la Vieja, of the five samples analyzed for isotopic content, all five plot directly in, or within error of, the magmatic degassing trend for speciation (Figure 6). Considering their isotopic content, all five exhibit secondary hydration and there is thus complete disagreement between the isotopic and speciation results. At Turrialba, three samples plot within the isotopic rehydration trend (Figure 5); considering the same three samples, two fall within the magmatic speciation trend while one sample falls above (Figure 6). Of the six Turrialba samples that fall within the magmatic degassing trend shown in Figure 5, four samples also fall within the magmatic degassing trend defined by speciation with two falling above it (Figure 6). The final two samples that fall above the degassing trend defined by speciation do not have corresponding isotopic data. Hence Turrialba shows partial disagreement between isotopic and speciation results.

Three samples from Turrialba were found to have exceptionally high values of OH/H_2O_{mol} (samples TA-1-6, TA-4-10 and TA-8-7; Table 3; Figure 6). All three samples contain molecular water values significantly below the average value for Turrialba and hydroxyl values near or above the average (Table 3). These findings may indicate the dominance of ion exchange as a mechanism for rehydration in these samples. Also of note is the significant error associated with these samples. The error is the result of the propagation of error as both OH and OH/H_2O are calculated values.

Given that the behaviour of hydrogen isotopes during secondary hydration is well documented, we believe that our findings in regard to speciation indicate that speciation is not an effective tool in distinguishing rehydration from magmatic degassing. We propose that this inconsistency arises from rehydration within hydrothermal systems as opposed to atmospheric conditions. At higher temperatures and pressures, hydration will proceed first by ion exchange with water soluble ions resulting in elevated OH followed by absorption of molecular water (Seligman et al., 2016 and references therein). Conversely, high proportions of H_2O_{mol} would be expected as slow cooling during ascent and storage drives the water speciation away from hydroxyl in favour of molecular water (Wysoczanski and Tani, 2006). These competing processes obscure speciation patterns, rendering them unreliable indicators of pre-eruptive hydration in hydrothermal environments. While speciation may effectively identify post-eruptive rehydration, it is not an effective tool in distinguishing pre-eruptive processes.

4.4 Secondary Hydration in Hydrothermal Conditions

Secondary hydration is typically studied as a post-eruptive process in atmospheric conditions (e.g., Seligman et al., 2018). In this study we consider rehydration as a pre-eruptive process wherein partially cooled and solidified magma is rehydrated within a hydrothermal system. This process occurs at higher temperatures and pressures, which alter the kinetics and mechanisms of hydration. The exact conditions within the hydrothermal systems of Turrialba and Rincón de la Vieja are unknown, but estimates can be made. At Rincón de la Vieja the crater lake has a maximum measured temperature of 55°C while fumarolic temperatures have

been measured up to 100°C, providing a minimum value for the hydrothermal system (Global Volcanism Program, 2017b, 2016). Turrialba does not host a crater lake, however previous studies have found the hydrothermal fluids at Turrialba to be 200-350°C (Mick et al., 2021). For the purpose of this study, we estimate minimum temperatures of 100-200°C and maximum temperatures of 350°C for both systems. Estimates of pressure are based on the lithostatic pressure and would likely not exceed a few megapascals.

We have argued herein that atmospheric speciation systematics do not hold in hydrothermal conditions, but that isotopic differentiation of primary and secondary water remains possible. In both cases our results show nearly complete degassing prior to any rehydration. This may be the result of slow magma ascent and shallow ponding of magma, as evidenced by phenocryst and microlite growth, allowing for more extensive degassing (Eichelberger et al., 1986; Castro and Mercer, 2004). Additionally, we have proposed that despite low water concentrations, samples from Rincón de la Vieja show significant isotopic change in terms of δD. Two related but distinct processes must be considered: (1) hydration of solid or semi-solid magma through incorporation of water i.e., secondary hydration, and (2) isotopic exchange between hydrogen in the solid or semi-solid magma and surrounding fluids, which may occur with or without significant changes in total water content. In hydrothermal environments, isotopic exchange can occur rapidly and may overprint primary magmatic signatures even in the absence of substantial hydration. During slow ascent, magma can reach equilibrium with confining pressures; in such cases δD can see a significant increase despite no notable increase in water content. Slow ascent from the magma chamber to the hydrothermal system allows for the interaction between the magma and isotopically heavy vapour from the deeper chamber (Giachetti et al., 2020). Additionally, at elevated temperatures (approximately 150°C) primary magmatic water in glass can exchange isotopically with secondary waters, again resulting in increasing δD values with little associated hydration (Anovitz et al., 2009). We propose that the elevated pressures and temperatures active within the hydrothermal system of Rincón de la Vieja allow for significant isotopic changes without significant hydration. This would account for the tight clustering of rehydrated Rincón de la Vieja samples (Figure 5). These findings are supported by experimental results from Giachetti et al. (2015) wherein glass showed enrichment in deuterium despite no significant water gain over 2 years at 70°C.

4.5 Compositional Controls on Rehydration

Composition has a known impact on rehydration, but such an effect is not reflected in our results. Previous work by Seligman et al. (2016) and Cassel and Breecker (2017) has found that felsic glass rehydrates at a faster rate than more mafic glass, 1500 years compared to over 7000 years at atmospheric conditions. Although rehydration in hydrothermal settings likely occurs more rapidly, the compositional control on rehydration rates remains valid (Seligman et al., 2016). Composition influences rehydration in two main ways. First, silica content increases polymerization which in turn increases H_2O solubility (Hudak and Bindeman, 2020). Second, rehydration requires a certain amount of porosity for fluid movement, a property again controlled by composition as higher-silica content results in higher viscosity, bubble retention and thus higher porosity (Giachetti et al., 2020; Nolan and Bindeman, 2013). This trend is not reflected in our findings. Considering samples found to have experienced secondary hydration, the more felsic Rincón de la Vieja samples contain 0.18 to 0.71 wt.% H_2O_{total}, while the more mafic Turrialba samples contain 1.30 to 2.29 wt.% H_2O_{total}. Although residence times may differ, they are likely of the same order of magnitude, and the observed differences in water content are more likely due to differing rehydration conditions between samples (e.g., Friedman and Long, 1976; Lowenstern and Pitcher, 2013).

4.6 The Source of Glass in Phreatic Eruptions

Turrialba and Rincón de la Vieja are active volcanoes of the Central American Volcanic Arc. Both systems experienced frequent activity over the course of this study, including phreatic and phreatomagmatic eruptions in addition to frequent gas burst at Rincón de la Vieja. As seen at other volcanoes globally, fresh glass has been identified at both systems including following eruptions classified as phreatic. This study has sought to determine if this glass is in fact juvenile, indicative of actively intruding magma, or if it has undergone secondary hydration, indicating a shallow, more passive magma.

This study has identified rehydrated glass at Rincón de la Vieja produced during eruptions between 2017 and 2021, and both fresh and rehydrated glass at Turrialba erupted between

2014 and 2022. During this period, repeated instances of incandescence at Turrialba were interpreted as the presence of shallow, active magma (Global Volcanism Program, 2018). The presence of fresh magmatic glass and incandescence at Turrialba support the conclusion of Alvarado et al. (2016) that a portion of the seemingly phreatic eruptions were in fact phreatomagmatic. Likewise, at Rincón de la Vieja, we attribute rehydrated glass to shallow magma stored within the hydrothermal systems which has been gradually cooling and solidifying. Mechanisms including dike and sill formation, degassing or eruption induced depressurization, buoyancy, and faulting could all result in small amounts of magma migrating upwards from the magma chamber into the hydrothermal system and then interacting with it. While such rehydration may also occur is the partially solidified material is erupted during phreatomagmatic eruptions, in cases where eruptions have been classified as phreatic, secondary hydration of pre-existing shallow magma provides a plausible mechanism for the observed occurrence of glass.

A proportion of the seemingly juvenile material examined in this study is, in fact, non-juvenile and has undergone secondary rehydration. We propose that this rehydrated, shallow-stored, likely semi-solid magma is passively entrained during phreatic eruptions, meaning it is fragmented by the eruption but does not drive it. However, this shallow magma, if sufficiently liquid, could also be erupted phreatomagmatically following depressurization caused by the failure of a hydrothermal seal and/or a preceding phreatic event. Our results indicate that this is a recurring process in both volcanic systems studied. These findings have important implications for how glassy material in explosive eruptions is currently interpreted, challenging the assumption that all such material is juvenile and indicative of phreatomagmatic activity.

5 Conclusions

This study investigates the origin of fresh-looking glass in eruptions classified as phreatic at Turrialba and Rincón de la Vieja volcanoes (Costa Rica), using hydrogen isotopes to distinguish between juvenile magmatic glass and rehydrated, passively entrained glass. Our results demonstrate that glass erupted during these events is not exclusively juvenile.

At Rincón de la Vieja, all analyzed glasses exhibit elevated δD values and low total water contents, inconsistent with magmatic degassing but consistent with secondary hydration by hydrothermal fluids similar to the crater lake. These findings support a model of passive entrainment as opposed to explosive fragmentation as an eruption driver. Turrialba presents a more complex scenario. Some samples follow the magmatic degassing trend and are interpreted as juvenile, while others show δD values (-99‰ and -104‰) and elevated H_2O_{total}, consistent with secondary hydration by hydrothermal fluids prior to eruption. The coexistence of both fresh and rehydrated glass within the same volcanic system highlights the variable nature of eruptive activity at Turrialba.

A key finding is the divergence between isotopic and water speciation data. Whereas hydrogen isotopes reliably distinguish between fresh and rehydrated glass, water speciation does not consistently reflect hydration history under hydrothermal conditions. This suggests that under elevated temperatures and pressures, typical of subsurface hydrothermal systems, the mechanisms and kinetics of hydration alter the speciation dynamics in ways that deviate from established atmospheric models limiting the reliability of speciation alone. Hydrogen isotopes therefore offer a more robust tool for reconstructing pre-eruptive processes while speciation requires further experimental calibration in hydrothermal conditions.

These findings have broad implications for volcanic hazard assessment and the classification of explosive eruptions. The identification of rehydrated glass in eruptions traditionally considered phreatic challenges the prevailing notion that the presence of juvenile-looking glass unequivocally indicates magmatic involvement. Our results suggest a need to revisit the current classification dichotomy between phreatic and phreatomagmatic eruptions. A spectrum-based classification is one way forward, ranging from phreatic (<1% fresh glass) to phreatomagmatic (50%), to magmatic (>99%), with intermediate “phreato-eruptions” (1-49%) showing mixed characteristics. Applying this model to eruptions at Turrialba and Rincón de la Vieja reclassifies most as intermediate phreato-eruptions, supporting the need for a more nuanced system. Such a classification is one possible example; a full and in-depth review of phreatic and phreatomagmatic eruptions would be necessary to accurately assign these types of boundaries.

Acknowledgements

The authors would like to thank Lang Shi and Justin Roman for their assistance with SEM and EPMA analysis. The authors also thank Jacob Lowenstern and Emily Johnson of the USGS for their assistance with FTIR analysis, and Brian Monteleone of the Woods Hole Oceanographic Institution for his assistance with SIMS analysis. This research was supported by a Canada Graduate Scholarship (Doctoral) from the Natural Sciences and Engineering Research Council to EM. This research was also supported by Discovery grants from the Natural Sciences and Engineering Research Council to JS. We are grateful to two anonymous reviewers for their helpful comments which improved the paper. We also thank the editor for their assistance with the paper.

Declaration of Interests

The authors declare they have no known competing financial interests or personal relationships that could have appeared to influence the work reported in this paper.

CRediT Statement

Emily Mick: Conceptualization, methodology, investigation, writing – original draft, visualization
Geoffroy Avard: Resources, writing – review and editing
John Stix: Conceptualization, methodology, resources, writing – review and editing, supervision

References

Alvarado, G.E., Kussmaul, S., Chiesa, S., Gillot, P.-Y., Appel, H., Wörner, G., Rundle, C., 1992. Resumen cronoestratigráfico de las rocas ígneas de Costa Rica basado en dataciones radiométricas. J. South Am. Earth Sci. 6, 151–168. https://doi.org/10.1016/0895-9811(92)90005-J

Alvarado, G.E., Mele, D., Dellino, P., de Moor, J.M., Avard, G., 2016. Are the ashes from the latest eruptions (2010–2016) at Turrialba volcano (Costa Rica) related to phreatic or

phreatomagmatic events? J. Volcanol. Geotherm. Res. 327, 407–415. https://doi.org/10.1016/j.jvolgeores.2016.09.003

Anovitz, L.M., Cole, D.R., Riciputi, L.R., 2009. Low-temperature isotopic exchange in obsidian: Implications for diffusive mechanisms. Geochim. Cosmochim. Acta 73, 3795–3806. https://doi.org/10.1016/j.gca.2009.02.035

Barberi, F., Bertagnini, A., Landi, P., Principe, C., 1992. A review on phreatic eruptions and their precursors. J. Volcanol. Geotherm. Res. 52, 231–246. https://doi.org/10.1016/0377-0273(92)90046-G

Battaglia, A., de Moor, J.M., Aiuppa, A., Avard, G., Bakkar, H., Bitetto, M., Mora Fernández, M.M., Kelly, P., Giudice, G., Delle Donne, D., Villalobos, H., 2019. Insights Into the Mechanisms of Phreatic Eruptions from Continuous High Frequency Volcanic Gas Monitoring: Rincón de la Vieja Volcano, Costa Rica. Front. Earth Sci. 6, 247. https://doi.org/10.3389/feart.2018.00247

Boudon, G., Rançon, J.-P., Kieffer, G., Soto, G., Traineau, H., Rossignol, J.-C., 1996. The 1966-1970 and 1991-1992 eruptions of Rincón de la Vieja volcano, Costa Rica: Example of the recurrent activity of a hydromagmatic system. Geomaterials. 322, 101-108.

Carr, M.J., 1984. Symmetrical and segmented variation of physical and geochemical characteristics of the Central American volcanic front. J. Volcanol. Geotherm. Res. 20, 231–252. https://doi.org/10.1016/0377-0273(84)90041-6

Cashman, K.V., Hoblitt, R., 2004. Magmatic precursors to the 18 May 1980 eruption of Mount St. Helens, USA. Geology 32, 141–144. https://doi.org/10.1130/G20078.1

Cassel, E.J., Breecker, D.O., 2017. Long-term stability of hydrogen isotope ratios in hydrated volcanic glass. Geochim. Cosmochim. Acta 200, 67–86. https://doi.org/10.1016/j.gca.2016.12.001

Castro, J.M., Mercer, C., 2004. Microlite textures and volatile contents of obsidian from the Inyo volcanic chain, California. Geophysical Research Letters 31, 2004GL020489. https://doi.org/10.1029/2004GL020489

Christenson, B.W., Reyes, A.G., Young, R., Moebis, A., Sherburn, S., Cole-Baker, J., Britten, K., 2010. Cyclic processes and factors leading to phreatic eruption events: Insights from the 25 September 2007 eruption through Ruapehu Crater Lake, New Zealand. J. Volcanol. Geotherm. Res. 191, 15–32. https://doi.org/10.1016/j.jvolgeores.2010.01.008

De Hoog, J.C.M., Taylor, B.E., Van Bergen, M.J., 2009. Hydrogen-isotope systematics in degassing basaltic magma and application to Indonesian arc basalts. Chem. Geol. 266, 256–266. https://doi.org/10.1016/j.chemgeo.2009.06.010

de Moor, J.M., Aiuppa, A., Avard, G., Wehrmann, H., Dunbar, N., Muller, C., Tamburello, G., Giudice, G., Liuzzo, M., Moretti, R., Conde, V., Galle, B., 2016. Turmoil at Turrialba Volcano (Costa Rica): Degassing and eruptive processes inferred from high-frequency gas monitoring. J. Geophys. Res. Solid Earth 121, 5761–5775. https://doi.org/10.1002/2016JB013150

Dobson, P.F., Epstein, S., Stolper, E.M., 1989. Hydrogen isotope fractionation between coexisting vapor and silicate glasses and melts at low pressure. Geochimica et Cosmochimica Acta 53, 2723–2730. https://doi.org/10.1016/0016-7037(89)90143-9

Eichelberger, J.C., Carrigan, C.R., Westrich, H.R., Price, R.H., 1986. Non-explosive silicic volcanism. Nature 323, 598–602. https://doi.org/10.1038/323598a0

Friedman, I., Long, W., 1976. Hydration Rate of Obsidian: New experimental techniques allow more precise dating of archeological and geological sites containing obsidian. Science 191, 347–352. https://doi.org/10.1126/science.191.4225.347

Friedman, I., Gleason, J., Sheppard, R.A., Gude, A.J., 2013a. Deuterium Fractionation as Water Diffuses into Silicic Volcanic Ash, in: Swart, P.K., Lohmann, K.C., Mckenzie, J., Savin, S. (Eds.), Geophysical Monograph Series. American Geophysical Union, Washington, D. C., pp. 321–323. https://doi.org/10.1029/GM078p0321

Friedman, I., Gleason, J., Warden, A., 2013b. Ancient Climate from Deuterium Content of Water in Volcanic Glass, in: Swart, P.K., Lohmann, K.C., Mckenzie, J., Savin, S. (Eds.), Geophysical Monograph Series. American Geophysical Union, Washington, D. C., pp. 309–319. https://doi.org/10.1029/GM078p0309

Germanovich, L.N., Lowell, R.P., 1995. The mechanism of phreatic eruptions. Journal of Geophysical Research 100, 8417–8434.

Giachetti, T., Gonnermann, H.M., Gardner, J.E., Shea, T., Gouldstone, A., 2015. Discriminating secondary from magmatic water in rhyolitic matrix-glass of volcanic pyroclasts using thermogravimetric analysis. Geochim. Cosmochim. Acta 148, 457–476. https://doi.org/10.1016/j.gca.2014.10.017

Giachetti, T., Hudak, M.R., Shea, T., Bindeman, I.N., Hoxsie, E.C., 2020. D/H ratios and H2O contents record degassing and rehydration history of rhyolitic magma and pyroclasts. Earth Planet. Sci. Lett. 530, 115909. https://doi.org/10.1016/j.epsl.2019.115909

Gilbert, J.S., Lane, S.J., 1994. The origin of accretionary lapilli. Bull. Volcanol. 56, 398–411. https://doi.org/10.1007/BF00326465

Global Volcanism Program, 2024. Report on Rincon de la Vieja (Costa Rica). Bull. Glob. Volcanism Netw. 49:1. https://doi.org/10.5479/si.GVP.BGVN202111-345020

Global Volcanism Program, 2023a. Report on Rincon de la Vieja (Costa Rica). Bull. Glob. Volcanism Netw. 48:7. https://doi.org/10.5479/si.GVP.BGVN202111-345020

Global Volcanism Program, 2023b. Report on Rincon de la Vieja (Costa Rica). Bull. Glob. Volcanism Netw. 48:1. https://doi.org/10.5479/si.GVP.BGVN202111-345020

Global Volcanism Program, 2022. Report on Rincon de la Vieja (Costa Rica). Bull. Glob. Volcanism Netw. 47. https://doi.org/10.5479/si.GVP.BGVN202111-345020

Global Volcanism Program, 2021. Report on Rincon de la Vieja (Costa Rica). Bull. Glob. Volcanism Netw. 46. https://doi.org/10.5479/si.GVP.BGVN202103-345020

Global Volcanism Program, 2020. Report on Rincon de la Vieja (Costa Rica). Bull. Glob. Volcanism Netw. 45. https://doi.org/10.5479/si.GVP.BGVN202010-345020

Global Volcanism Program, 2018. Report on Turrialba (Costa Rica). Bull. Glob. Volcanism Netw. 43. https://doi.org/10.5479/si.GVP.BGVN201809-345070

Global Volcanism Program, 2017a. Report on Turrialba (Costa Rica). Bull. Glob. Volcanism Netw. 42. https://doi.org/10.5479/si.GVP.BGVN201706-345070

Global Volcanism Program, 2017b. Report on Rincon de la Vieja (Costa Rica). Bull. Glob. Volcanism Netw. 42. https://doi.org/10.5479/si.GVP.BGVN201708-345020

Global Volcanism Program, 2016. Report on Rincon de la Vieja (Costa Rica). Bull. Glob. Volcanism Netw. 41. https://doi.org/10.5479/si.GVP.BGVN201601-345020

Global Volcanism Program, 2015. Report on Turrialba (Costa Rica). Bull. Glob. Volcanism Netw. 40. https://doi.org/10.5479/si.GVP.BGVN201504-345070

Hammer, J., Cashman, K.V., Hoblitt, R., Newman, S., 1999. Degassing and microlite crystallization during pre-climactic events of the 1991 eruption of Mt. Pinatubo, Philippines. Bull. Volcanol. 60, 355–380. https://doi.org/10.1007/s004450050238

Heap, M.J., Kennedy, B.M., Farquharson, J.I., Ashworth, J., Mayer, K., Letham-Brake,

M., Reuschlé, T., Gilg, H.A., Scheu, B., Lavallée, Y., Siratovich, P., Cole, J., Jolly, A.D., Baud, P., Dingwell, D.B., 2017. A multidisciplinary approach to quantify the permeability of the Whakaari/White Island volcanic hydrothermal system (Taupo Volcanic Zone, New Zealand). J. Volcanol. Geotherm. Res. 332, 88–108. https://doi.org/10.1016/j.jvolgeores.2016.12.004

Hudak, M.R., Bindeman, I.N., 2020. Solubility, diffusivity, and O isotope systematics of H_2O in rhyolitic glass in hydrothermal temperature experiments. Geochim. Cosmochim. Acta 283, 222–242. https://doi.org/10.1016/j.gca.2020.06.009

Hudak, M.R., Bindeman, I.N., Watkins, J.M., Lowenstern, J.B., 2022. Hydrogen isotope behavior during rhyolite glass hydration under hydrothermal conditions. Geochim. Cosmochim. Acta 337, 33–48. https://doi.org/10.1016/j.gca.2022.09.032

Hudak, M.R., Bindeman, I.N., Loewen, M.W., Giachetti, T., 2021. Syn-Eruptive Hydration of Volcanic Ash Records Pyroclast-Water Interaction in Explosive Eruptions. Geophysical Research Letters 48, e2021GL094141. https://doi.org/10.1029/2021GL094141

IAEA/WMO (2015). Global Network of Isotopes in Precipitation. The GNIP Database.

Ihinger, P.D., Zhang, Y., Stolper, E.M., 1999. The speciation of dissolved water in rhyolitic melt. Geochimica et Cosmochimica Acta 63, 3567–3578. https://doi.org/10.1016/S0016-7037(99)00277-X

Kaneko, T., Maeno, F., Nakada, S., 2016. 2014 Mount Ontake eruption: characteristics of the phreatic eruption as inferred from aerial observations. Earth Planets Space 68, 72. https://doi.org/10.1186/s40623-016-0452-y

Le Bas, M.J.L., Maitre, R.W., Streckeisen, A., Zanettin, B., IUGS Subcommission on the Systematics of Igneous Rocks, 1986. A Chemical Classification of Volcanic Rocks Based on the Total Alkali-Silica Diagram. Journal of Petrology 27, 745–750. https://doi.org/10.1093/petrology/27.3.745

Lowenstern, J.B., Pitcher, B.W., 2013. Analysis of H2O in silicate glass using attenuated total reflectance (ATR) micro-FTIR spectroscopy. Am. Mineral. 98, 1660–1668. https://doi.org/10.2138/am.2013.4466

Lube, G., Breard, E.C.P., Cronin, S.J., Procter, J.N., Brenna, M., Moebis, A., Pardo, N., Stewart, R.B., Jolly, A., Fournier, N., 2014. Dynamics of surges generated by hydrothermal blasts during the 6 August 2012 Te Maari eruption, Mt. Tongariro, New Zealand. J. Volcanol. Geotherm. Res. 286, 348–366. https://doi.org/10.1016/j.jvolgeores.2014.05.010

Martin, E., Bindeman, I., Balan, E., Palandri, J., Seligman, A., Villemant, B., 2017. Hydrogen isotope determination by TC/EA technique in application to volcanic glass as a window into secondary hydration. J. Volcanol. Geotherm. Res. 348, 49–61. https://doi.org/10.1016/j.jvolgeores.2017.10.013

Martini, F., Tassi, F., Vaselli, O., Del Potro, R., Martinez, M., del Laat, R.V., Fernandez, E., 2010. Geophysical, geochemical and geodetical signals of reawakening at Turrialba volcano (Costa Rica) after almost 150 years of quiescence. J. Volcanol. Geotherm. Res. 198, 416–432. https://doi.org/10.1016/j.jvolgeores.2010.09.021

Mick, E., Stix, J., de Moor, J.M., Avard, G., 2021. Hydrothermal alteration and sealing at Turrialba volcano, Costa Rica, as a mechanism for phreatic eruption triggering. J. Volcanol. Geotherm. Res. 416, 107297. https://doi.org/10.1016/j.jvolgeores.2021.107297

Miyagi, I., Geshi, N., Hamasaki, S., Oikawa, T., Tomiya, A., 2020. Heat source of the 2014 phreatic eruption of Mount Ontake, Japan. Bull. Volcanol. 82, 33. https://doi.org/10.1007/s00445-020-1358-x

Newman, S., Epstein, S., Stolper, E., 1988. Water, carbon dioxide, and hydrogen isotopes in glasses from the ca. 1340 A.D. eruption of the Mono Craters, California: Constraints on degassing phenomena and initial volatile content. J. Volcanol. Geotherm. Res. 35, 75–96. https://doi.org/10.1016/0377-0273(88)90007-8

Newman, S., Lowenstern, J.B., 2002. VolatileCalc: a silicate melt–H2O–CO2 solution model written in Visual Basic for excel. Computers & Geosciences 28, 597–604. https://doi.org/10.1016/S0098-3004(01)00081-4

Nolan, G.S., Bindeman, I.N., 2013. Experimental investigation of rates and mechanisms of isotope exchange (O, H) between volcanic ash and isotopically-labeled water. Geochim. Cosmochim. Acta 111, 5–27. https://doi.org/10.1016/j.gca.2013.01.020

Pardo, N., Cronin, S.J., Németh, K., Brenna, M., Schipper, C.I., Breard, E., White, J.D.L., Procter, J., Stewart, B., Agustín-Flores, J., Moebis, A., Zernack, A., Kereszturi, G., Lube, G., Auer, A., Neall, V., Wallace, C., 2014. Perils in distinguishing phreatic from phreatomagmatic ash; insights into the eruption mechanisms of the 6 August 2012 Mt. Tongariro eruption, New Zealand. J. Volcanol. Geotherm. Res. 286, 397–414. https://doi.org/10.1016/j.jvolgeores.2014.05.001

Pearce, J.A., Peate, D.W., 1995. Tectonic Implications of the Composition of Volcanic ARC Magmas. Annu. Rev. Earth Planet. Sci. 23, 251–285. https://doi.org/10.1146/annurev.ea.23.050195.001343

Reagan, M., Duarte, E., Soto, G.J., Fernandez, E., 2006. The eruptive history of Turrialba volcano, Costa Rica, and potential hazards from future eruptions. Geol. Soc. Am. Spec. Pap. 235–253. https://doi.org/10.1130/2006.2412(13)

Romero, J.E., Aguilera, F., Delgado, F., Guzmán, D., Van Eaton, A.R., Luengo, N., Caro, J., Bustillos, J., Guevara, A., Holbik, S., Tormey, D., Zegarra, I., 2020. Combining ash analyses with remote sensing to identify juvenile magma involvement and fragmentation mechanisms during the 2018/19 small eruption of Peteroa volcano (Southern Andes). J. Volcanol. Geotherm. Res. 402, 106984. https://doi.org/10.1016/j.jvolgeores.2020.106984

Sánchez-Murillo, R., Birkel, C., Welsh, K., Esquivel-Hernández, G., Corrales-Salazar, J., Boll, J., Brooks, E., Roupsard, O., Sáenz-Rosales, O., Katchan, I., Arce-Mesén, R., Soulsby, C., Araguás-Araguás, L.J., 2016. Key drivers controlling stable isotope variations in daily precipitation of Costa Rica: Caribbean Sea versus Eastern Pacific Ocean moisture sources. Quat. Sci. Rev. 131, 250–261. https://doi.org/10.1016/j.quascirev.2015.08.028

Seligman, A.N., Bindeman, I., Van Eaton, A., Hoblitt, R., 2018. Isotopic insights into the degassing and secondary hydration of volcanic glass from the 1980 eruptions of Mount St. Helens. Bull. Volcanol. 80, 37. https://doi.org/10.1007/s00445-018-1212-6

Seligman, A.N., Bindeman, I.N., Watkins, J.M., Ross, A.M., 2016. Water in volcanic glass: From volcanic degassing to secondary hydration. Geochim. Cosmochim. Acta 191, 216–238. https://doi.org/10.1016/j.gca.2016.07.010

Shaw, A.M., Hauri, E.H., Fischer, T.P., Hilton, D.R., Kelley, K.A., 2008. Hydrogen isotopes in Mariana arc melt inclusions: Implications for subduction dehydration and the deep-Earth water cycle. Earth and Planetary Science Letters 275, 138–145. https://doi.org/10.1016/j.epsl.2008.08.015

Silver, L., Stolper, E., 1989. Water in Albitic Glasses. Journal of Petrology 30, 667–709. https://doi.org/10.1093/petrology/30.3.667

Stix, J., de Moor, J.M., 2018. Understanding and forecasting phreatic eruptions driven by magmatic degassing. Earth Planets Space Online Heidelb. 70, 1–19. http://dx.doi.org/10.1186/s40623-018-0855-z

Tassi, F., Vaselli, O., Fernandez, O., Duarte, E., Martinez, M., Delgado Huertas, A., Bergamaschi, F., 2009. Morphological and geochemical features of crater lakes in Costa Rica: an overview. J. Limnol. 68. https://doi.org/10.3274/jl09-68-2-04

Taylor, B.E., Eichelberger, J.C., Westrich, H.R., 1983. Hydrogen isotopic evidence of rhyolitic magma degassing during shallow intrusion and eruption. Nature 306, 541–545. https://doi.org/10.1038/306541a0

Vaselli, O., Tassi, F., Duarte, E., Fernandez, E., Poreda, R.J., Huertas, A.D., 2010. Evolution of fluid geochemistry at the Turrialba volcano (Costa Rica) from 1998 to 2008. Bull Volcanol 72, 397–410. https://doi.org/10.1007/s00445-009-0332-4

Wysoczanski, R., Tani, K., 2006. Spectroscopic FTIR imaging of water species in silicic volcanic glasses and melt inclusions: An example from the Izu-Bonin arc. J. Volcanol. Geotherm. Res. 156, 302–314. https://doi.org/10.1016/j.jvolgeores.2006.03.024

Zhang, Y., Stolper, E.M., Wasserburg, G.J., 1991. Diffusion of water in rhyolitic glasses. Geochimica et Cosmochimica Acta 55, 441–456. https://doi.org/10.1016/0016-7037(91)90003-N

Figures

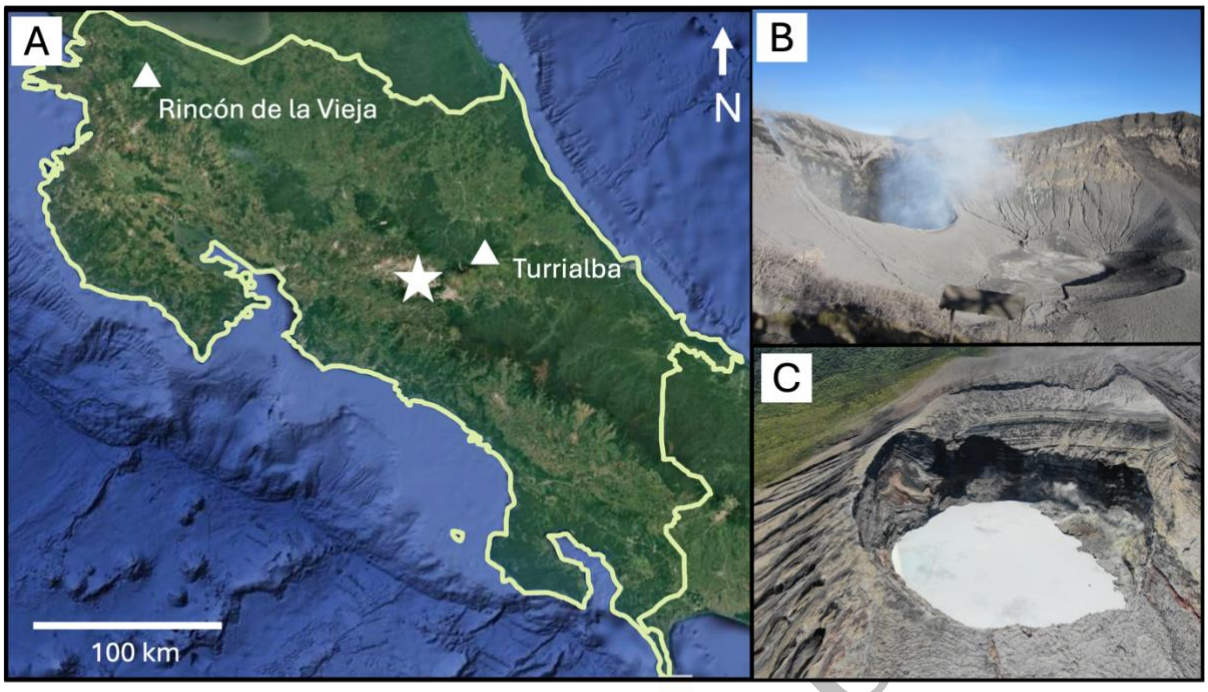

Figure 1

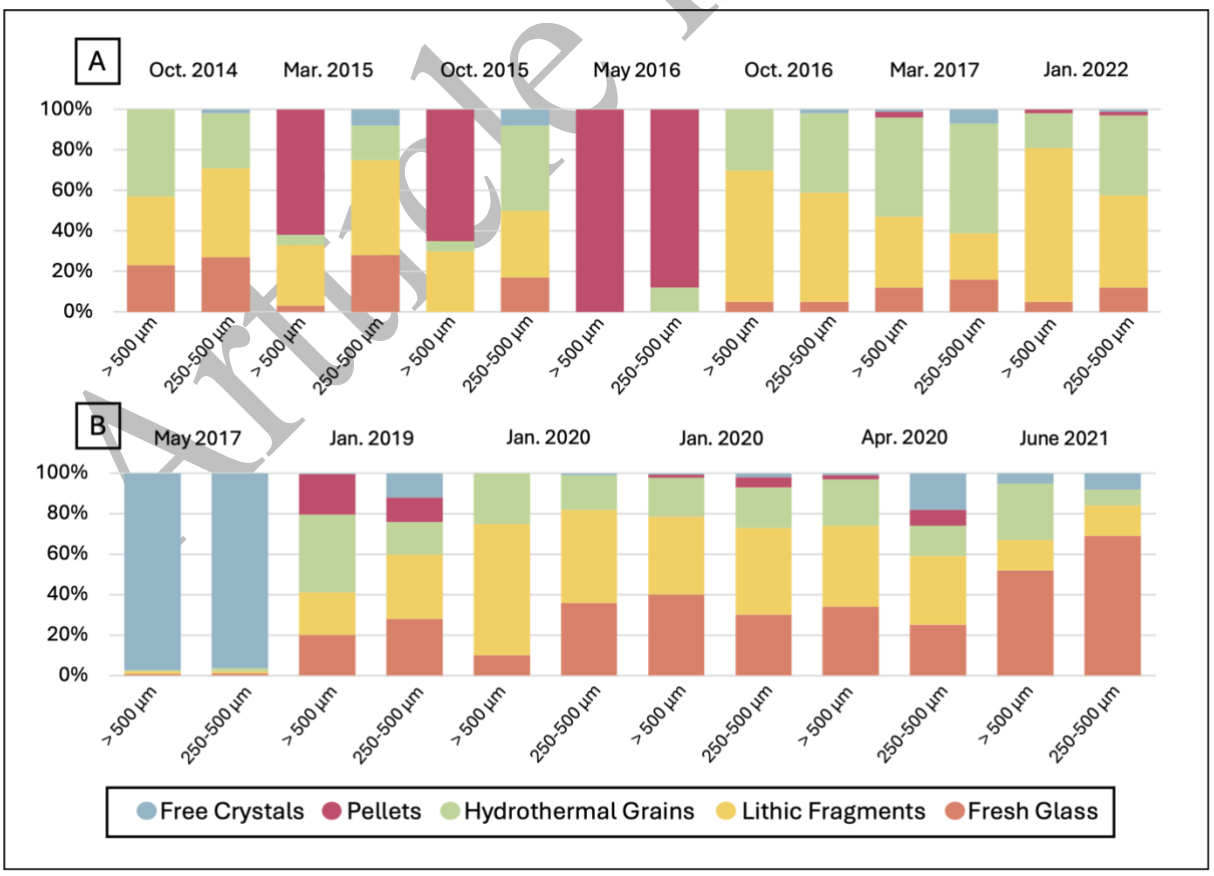

Figure 2

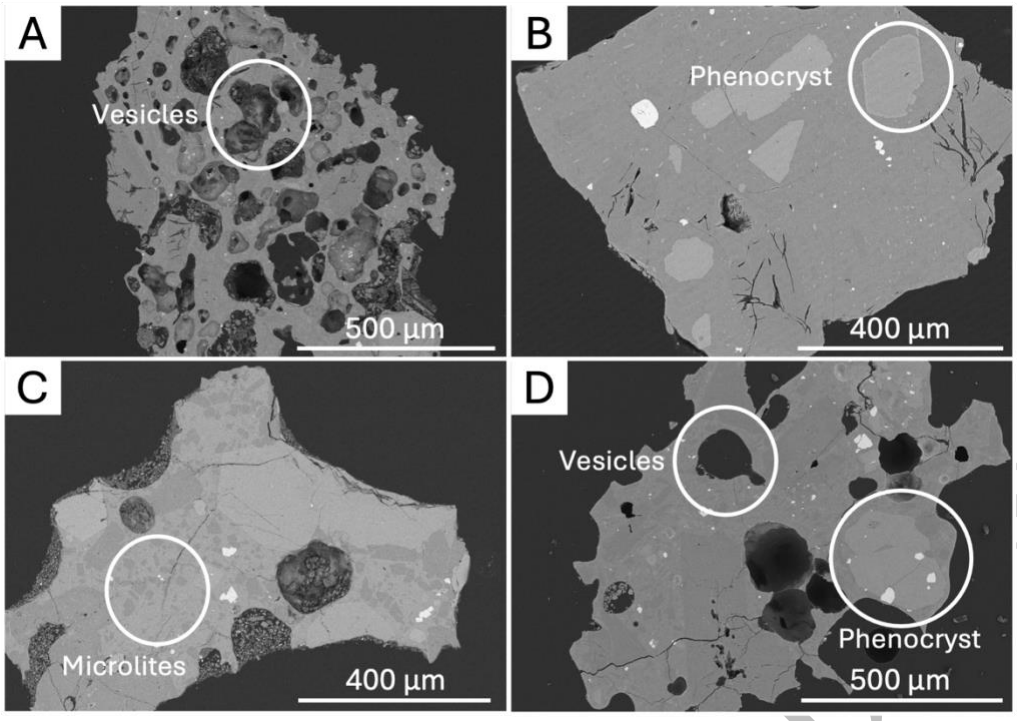

Figure 3

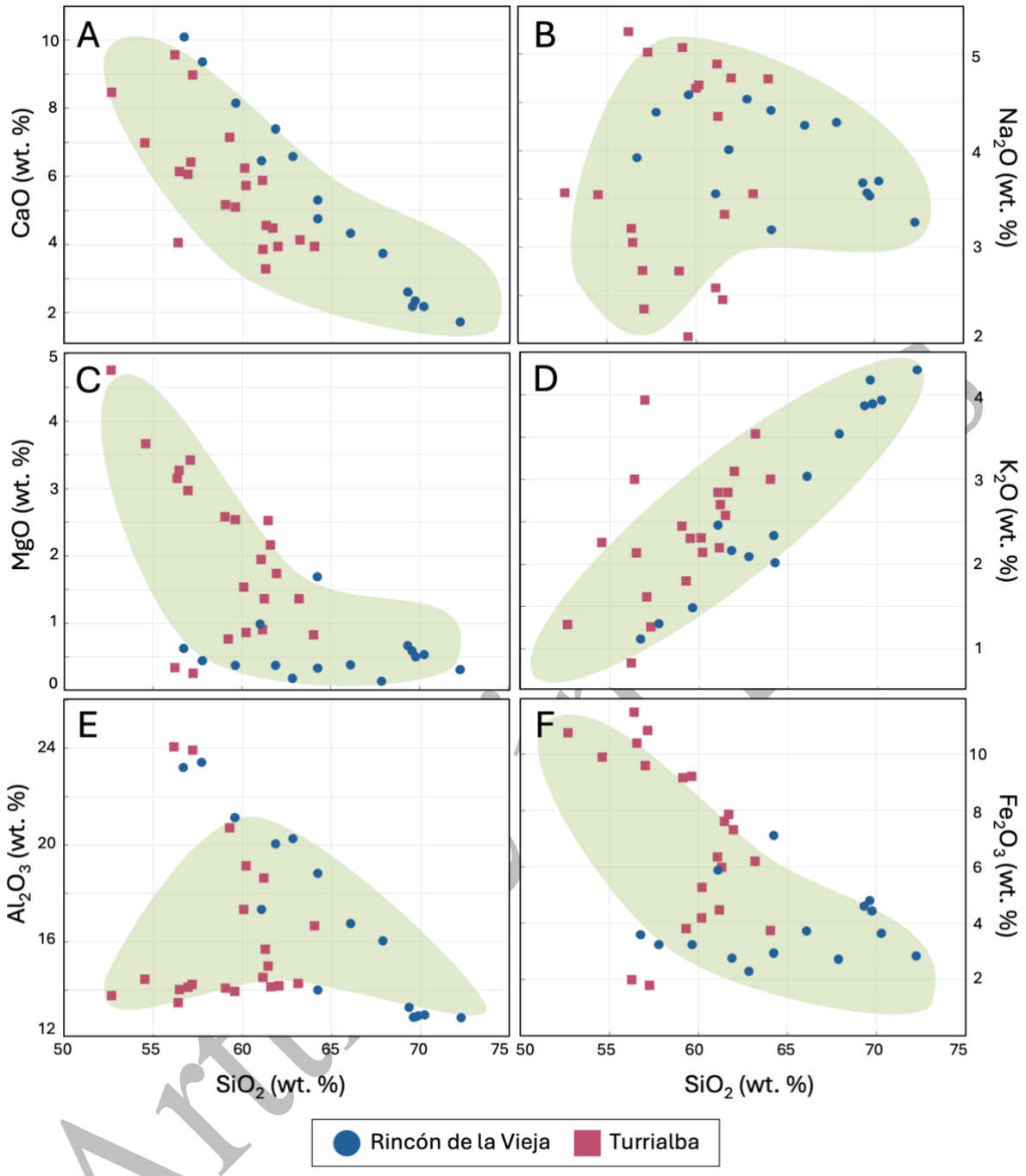

Figure 4

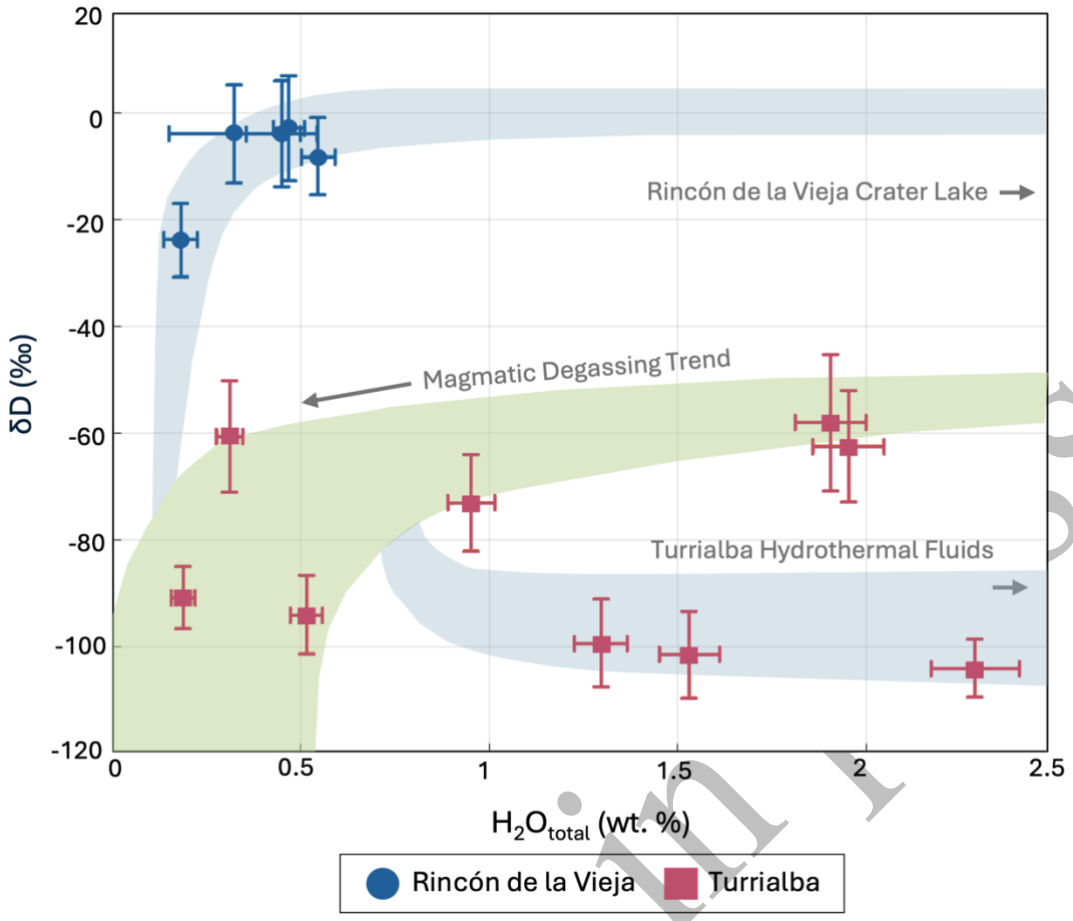

Figure 5

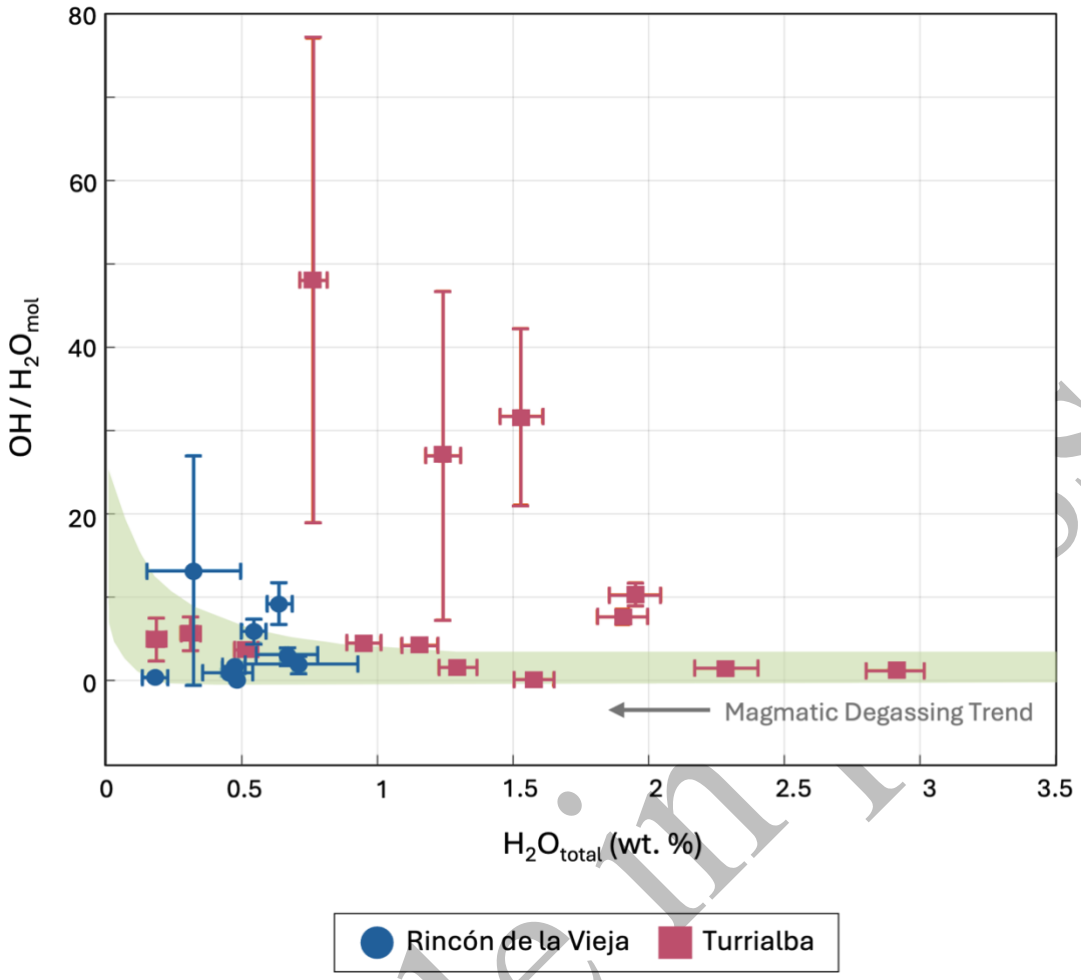

Figure 6

Table 1

Sample	Size Fraction	Glass	Lithics	Hydrothermal	Pellets	Crystals
RA-1	>500 µm	1	1	1	0	97
RA-1	250-500 µm	1	1	2	0	96
RA-2	>500 µm	20	22	38	20	0
RA-2	250-500 µm	28	32	16	12	12
RA-3	>500 µm	40	38	19	2	1
RA-3	250-500 µm	30	43	20	5	2
RA-4	>500 µm	34	40	23	2	1
RA-4	250-500 µm	25	34	15	8	18
RA-5	>500 µm	10	65	25	0	0
RA-5	250-500 µm	36	46	17	0	1
RA-6	>500 µm	52	15	28	0	5
RA-6	250-500 µm	69	15	8	0	8
TA-1	>500 µm	23	34	43	0	0
TA-1	250-500 µm	27	44	27	0	2
TA-3	>500 µm	3	30	5	62	0
TA-3	250-500 µm	28	47	17	0	8
TA-4	>500 µm	0	30	5	65	0
TA-4	250-500 µm	17	33	42	0	8
TA-6	>500 µm	0	0	0	100	0
TA-6	250-500 µm	0	0	12	88	0
TA-7	>500 µm	5	65	30	0	0
TA-7	250-500 µm	5	54	39	0	2
TA-8	>500 µm	12	35	49	3	1
TA-8	250-500 µm	16	23	54	0	7
TA-9	>500 µm	5	76	17	2	0
TA-9	250-500 µm	12	46	39	2	1

Table 2

Sample	SiO_2 (wt. %)	TiO_2 (wt. %)	Al_2O_3 (wt. %)	Fe_2O_3 (wt. %)	MnO (wt. %)	MgO (wt. %)	CaO (wt. %)	Na_2O (wt. %)	K_2O (wt. %)	Total
RA-2-1	56.70	0.59	23.22	3.60	0.12	0.63	10.09	3.92	1.11	99.98
RA-2-2	61.07	0.96	17.33	5.85	0.19	0.95	6.44	3.55	2.47	98.81
RA-3-3	59.62	0.58	21.12	3.23	0.10	0.38	8.13	4.59	1.49	99.24
RA-3-9	69.33	0.74	13.26	4.60	0.10	0.67	2.59	3.67	3.87	98.85
RA-3-10	69.61	0.80	12.90	4.77	0.10	0.58	2.19	3.56	4.18	98.69
RA-3-11	57.74	0.40	23.42	3.22	0.16	0.44	9.35	4.40	1.30	100.44
RA-4-5	62.83	0.37	20.26	2.26	0.00	0.20	6.57	4.54	2.09	99.11
RA-4-11	66.07	0.52	16.72	3.71	0.10	0.39	4.33	4.27	3.05	99.18
RA-5-5	64.25	0.97	13.99	7.11	0.15	1.69	4.78	3.18	2.01	98.13
RA-6-1	70.25	0.62	12.94	3.61	0.11	0.53	2.16	3.69	3.94	97.85
RA-6-2	64.22	0.54	18.82	2.90	0.00	0.33	5.31	4.42	2.34	98.87
RA-6-3	67.87	0.61	16.03	2.70	0.00	0.13	3.72	4.30	3.53	98.89
RA-6-4	72.24	0.84	12.86	2.81	0.09	0.31	1.73	3.27	4.30	98.43
RA-6-6	69.73	0.77	12.87	4.42	0.00	0.53	2.35	3.53	3.90	98.08
RA-6-8	61.85	0.67	20.04	2.75	0.00	0.37	7.36	4.01	2.16	99.21
TA-1-3	56.96	1.91	14.07	9.56	0.14	2.95	6.09	2.75	3.93	98.37
TA-1-6	59.07	1.95	14.06	9.13	0.14	2.56	5.18	2.76	2.45	97.31
TA-1-7	57.08	2.01	14.13	10.82	0.17	3.41	6.40	2.36	1.61	97.99
TA-2-2	56.21	0.40	24.07	1.99	0.00	0.34	9.55	5.23	0.83	98.63
TA-2-1	61.25	1.34	15.67	5.99	0.11	1.35	3.27	4.35	2.72	96.04
TA-2-8	64.05	1.00	16.62	3.70	0.12	0.83	3.92	4.74	3.00	97.98
TA-3-7	63.19	1.50	14.23	6.13	0.13	1.36	4.10	3.54	3.53	97.72
TA-3-8	61.61	1.47	14.14	7.81	0.14	2.14	4.50	3.34	2.85	98.00
TA-3-12	52.64	2.77	13.76	10.73	0.14	4.76	8.45	3.56	1.28	98.09
TA-3-13	54.53	2.18	14.42	9.85	0.14	3.66	7.00	3.54	2.25	97.57
TA-4-2	61.08	1.21	14.52	6.32	0.11	1.93	3.82	2.58	2.85	94.40
TA-4-10	59.56	1.84	13.91	9.18	0.16	2.54	5.08	2.07	2.31	96.65
TA-7-2	56.39	2.07	13.49	11.45	0.16	3.15	4.08	3.19	3.00	96.98
TA-7-4	61.47	1.32	15.00	7.64	0.15	2.51	4.51	2.46	2.57	97.63
TA-7-5	56.47	2.00	14.02	10.37	0.17	3.28	6.11	3.04	2.14	97.61
TA-8-1	60.19	1.17	19.14	4.14	0.14	0.86	6.27	4.68	2.13	98.73
TA-8-2	61.15	0.99	18.61	4.43	0.12	0.92	5.88	4.90	2.19	99.19
TA-8-3	60.13	1.13	17.34	5.29	0.13	1.53	5.76	4.66	2.31	98.26
TA-8-7	61.98	1.53	14.13	7.31	0.14	1.74	3.90	4.75	3.10	98.57
TA-8-9	59.25	0.83	20.70	3.82	0.13	0.77	7.11	5.08	1.79	99.47
TA-8-10	57.25	0.36	23.91	1.79	0.00	0.25	8.99	5.01	1.27	98.84

Table 3

Sample	H_2O_{Total} (wt. %)	H_2O_{mol} (wt. %)	OH (wt. %)	δD (‰)
RA-2-1	0.55 ± 0.04	0.08 ± 0.02	0.47 ± 0.05	-8 ± 7
RA-3-9	0.47 ± 0.04	0.19 ± 0.02	0.28 ± 0.05	-3 ± 10
RA-3-10	0.48 ± 0.01	0.41 ± 0.05	0.07 ± 0.04	
RA-4-5	0.45 ± 0.09	0.23 ± 0.08	0.22 ± 0.04	-4 ± 10
RA-5-5	0.64 ± 0.05	0.06 ± 0.02	0.58 ± 0.05	
RA-6-1	0.18 ± 0.05	0.13 ± 0.04	0.05 ± 0.01	-24 ± 7
RA-6-2	0.33 ± 0.18	0.02 ± 0.02	0.30 ± 0.15	-4 ± 9
RA-6-4	0.71 ± 0.22	0.24 ± 0.10	0.47 ± 0.15	
RA-6-6				-27 ± 8
RA-6-8	0.67 ± 0.11	0.16 ± 0.02	0.51 ± 0.10	
TA-1-3	0.52 ± 0.04	0.11 ± 0.02	0.41 ± 0.05	-94 ± 7
TA-1-6	1.53 ± 0.08	0.05 ± 0.02	1.48 ± 0.08	-102 ± 8
TA-1-7	1.30 ± 0.07	0.48 ± 0.04	0.81 ± 0.08	-99 ± 8
TA-3-12	2.91 ± 0.11	1.27 ± 0.07	1.64 ± 0.13	
TA-4-2	1.58 ± 0.07	1.38 ± 0.08	0.20 ± 0.10	
TA-4-10	1.24 ± 0.06	0.04 ± 0.03	1.20 ± 0.07	
TA-7-2	0.19 ± 0.03	0.03 ± 0.01	0.16 ± 0.03	-91 ± 6
TA-7-5	2.29 ± 0.12	0.91 ± 0.28	1.38 ± 0.40	-104 ± 5
TA-8-1	1.16 ± 0.07	0.22 ± 0.02	0.94 ± 0.07	
TA-8-2	0.31 ± 0.04	0.05 ± 0.02	0.27 ± 0.04	-61 ± 10
TA-8-3	0.95 ± 0.06	0.17 ± 0.02	0.78 ± 0.07	-73 ± 9
TA-8-7	0.77 ± 0.05	0.02 ± 0.01	0.75 ± 0.05	
TA-8-9	1.95 ± 0.09	0.17 ± 0.02	1.78 ± 0.10	-62 ± 10
TA-8-10	1.91 ± 0.09	0.22 ± 0.02	1.69 ± 0.10	-58 ± 13

Captions

Figure 1 A) Map depicting locations of Rincón de la Vieja and Turrialba volcanoes within Costa Rica. The capital city of Costa Rica, San José is identified by a star. B) Photo of the active crater of Turrialba. C) View of the active crater of Rincón de la Vieja.

Figure 2 Grain type abundances for ashes from A) Turrialba between October 2014 and January 2022, and B) Rincón de la Vieja between May 2017 and June 2021. Data determined by grain counting using categories set out in Romero et al. (2020).

Figure 3 Examples of typical glassy grains analyzed. A) Highly vesicular glass grain with microlites, sample RA-2-1. B) Blocky glass grain with small phenocrysts, sample RA-3-9. C) Moderately vesicular glass with phenocrysts, sample TA-7-2. D) Vesicular glassy grain with phenocrysts and microlites, sample TA-8-7.

Figure 4 Harker diagrams for glass grains from Rincón de la Vieja (blue) and Turrialba (red) volcanoes. Magmatic trends are shown in green. All data measured using EPMA.

Figure 5 Total water (wt. %) versus hydrogen isotopic ratio (‰) for glassy ash grains from Rincón de la Vieja (blue) and Turrialba (red) volcanoes. Magmatic degassing trend proposed by Taylor et al. (1893) is shown in green plotted using data presented in Giachetti et al. (2020), Newman et al. (1988) and Taylor et al. (1983). Secondary hydration trends are shown in blue with Turrialba fumarolic isotopic data from Vaselli et al. (2010) and Rincón de la Vieja crater lake isotopic data from Tassi et al. (2009). Total water measured using FTIR-ATR, δD measured using SIMS.

Figure 6 Total water (wt. %) versus water speciation ratio for glassy ash grains from Rincón de la Vieja (blue) and Turrialba (red) volcanoes. Magmatic degassing trend is shown in green adapted from Giachetti et al. (2020) and Newman et al. (1988). All data measured using FTIR-ATR.

Table 1 Summary of componentry data for Rincón de la Vieja (RA) and Turrialba (TA) ash samples. Proportions of each component are in percentages.

Table 2 Major element oxide data for Rincón de la Vieja (RA) and Turrialba (TA) glassy ash grains. Values are unnormalized averages for each sample; full data is available in supplementary material Tables 1-2. Data obtained by EPMA.

Table 3 Total water, water speciation and deuterium/hydrogen isotopic ratio data for glassy ash grains from Rincón de la Vieja (RA) and Turrialba (TA). Total water and speciation data obtained by FTIR-ATR; isotopic data obtained by SIMS. Values are averages for each sample; full data, standards and calibration curves are available in the supplementary materials Figures 1-3 and Tables 3-6.